UvrD facilitates DNA repair by pulling RNA polymerase backwards

Vitaly Epshtein[1,*], **Venu Kamarthapu**[1,2,*], **Katelyn McGary**[1], **Vladimir Svetlov**[1], **Beatrix Ueberheide**[1], **Sergey Proshkin**[3], **Alexander Mironov**[3,4], and **Evgeny Nudler**[1,2]

[1]Department of Biochemistry and Molecular Pharmacology, New York University School of Medicine, New York, New York 10016, USA

[2]Howard Hughes Medical Institute, New York University School of Medicine, New York, New York 10016, USA

[3]State Research Institute of Genetics and Selection of Industrial Microorganisms, Moscow 117545, Russia

[4]Engelhardt Institute of Molecular Biology, Russian Academy of Science, Moscow 119991, Russia

Abstract

UvrD helicase is required for nucleotide excision repair, although its role in this process is not well defined. Here we show that *Escherichia coli* UvrD binds RNA polymerase during transcription elongation and, using its helicase/translocase activity, forces RNA polymerase to slide backward along DNA. By inducing backtracking, UvrD exposes DNA lesions shielded by blocked RNA polymerase, allowing nucleotide excision repair enzymes to gain access to sites of damage. Our results establish UvrD as a bona fide transcription elongation factor that contributes to genomic integrity by resolving conflicts between transcription and DNA repair complexes. We further show that the elongation factor NusA cooperates with UvrD in coupling transcription to DNA repair by promoting backtracking and recruiting nucleotide excision repair enzymes to exposed lesions. Because backtracking is a shared feature of all cellular RNA polymerases, we propose that this mechanism enables RNA polymerases to function as global DNA damage scanners in bacteria and eukaryotes.

Nucleotide excision repair (NER) is the most versatile and evolutionarily conserved mechanism used by prokaryotic and eukaryotic cells to repair diverse types of DNA lesions[1,2]. In bacteria, the general NER pathway commences when UvrA/UvrB proteins bind damaged DNA and recruit UvrC to cleave the impaired strand on both sides of the

lesion. The resulting oligonucleotide is displaced by UvrD and/or DNA polymerase I, which fills the gap using the complementary strand as a template[2–4].

NER rates are usually greatest at transcriptionally active genes. Moreover, the transcribed DNA strand is preferentially repaired compared to the non-transcribed strand[5]. This phenomenon, known as transcription-coupled repair (TCR), is a sub-pathway of global NER[3,6]. The current model of bacterial TCR postulates that a DNA lesion blocking the progression of the transcription elongation complex is shielded from NER enzymes by the stalled RNAP. The DNA translocase, Mfd, binds to the stalled EC through the β subunit of RNA polymerase (RNAP) and dislodges the complex by 'pushing' it forward[7–10]. Concurrently, Mfd recruits UvrA to the exposed lesion site to expedite NER[10].

Here we propose an alternative TCR model whose key component is UvrD, a member of DNA helicase superfamily 1, which translocates in a 3′ to 5′ direction using a single-strand, DNA-dependent, ATPase activity[11–13]. In contrast to Mfd, UvrD facilitates NER by pulling RNAP backward from the DNA lesion without causing termination. Our model further explains the role of elongation factor NusA, which is known to contribute to Mfd-independent TCR[14]. In this model RNAP recruits the NER complex via UvrD/NusA to the damage site.

UvrD binds RNAP *in vitro* and *in vivo*

We performed a mass spectrometry (MS)-assisted survey of proteins that interact with *E. coli* RNAP *in vivo* by treating *E. coli* K12 MG1655 cultures with formaldehyde and isolated RNAP-containing material. Peptides in this material were identified by tandem liquid chromatography mass spectrometry (LC-MS/MS) and used to calculate an exponentially modified protein abundance index (emPAI). This label-free method estimates the relative amount of proteins by the number of sequenced peptides per protein compared with the number of theoretically observable peptides[15]. UvrD appeared in RNAP crosslinked complexes in abundance comparable to that of bona fide transcription elongation/termination factors NusA, NusG or Rho (Extended Data Fig. 1), indicating a potential direct interaction between UvrD and RNAP.

To verify that UvrD, interacts with RNAP directly, we performed *in vitro* pull-down assays with purified UvrD and His6-tagged RNAP adsorbed to metal-chelating beads. UvrD bound to the beads only in the presence of immobilized RNAP and remained bound through multiple washings (Extended Data Fig. 1b). The UvrD–RNAP core complex was also isolated in a major discrete peak by size-exclusion chromatography (Extended Data Fig. 1c). Collectively, these data demonstrate stable and specific binding of UvrD to RNAP.

UvrD promotes RNAP backtracking

To investigate the role of UvrD in transcription we reconstituted a single-round runoff assay that measured 'walking' (NTP supply-controlled elongation) of the elongation complex along DNA[16]. We observed little effect of UvrD on RNAP promoter binding and open complex formation (not shown); however, UvrD dramatically influenced elongation, interrupting transcription at many positions along the template, so that only a fraction of

elongation complexes produced a full-length (runoff) transcript (Fig. 1a, lane 2). Some UvrD-induced transcriptional 'arrests' coincided with pre-existing pause sites, whereas others formed *de novo*. Most did not change significantly with time, indicating that the corresponding elongation complexes were either permanently arrested or terminated by UvrD. We excluded the latter possibility by showing that the majority of those transcripts remained bound to RNAP after extensive washing with high-salt buffer (Fig. 1a, lane 3).

Most transcriptional pauses and arrests are caused by backtracking—a reverse sliding of RNAP along DNA and RNA[17]. In bacteria, backtracked RNAP is prone to transcript cleavage stimulated by Gre factors, which reactivate elongation complexes by removing the extruding 3′ portion of the nascent RNA[18,19]. To test whether elongation complexes arrested by UvrD were backtracked, we first washed them to remove unincorporated NTPs and UvrD, and incubated with GreB (Fig. 1a, lane 4). GreB shortened most of the transcripts from UvrD-arrested elongation complexes and reactivated these complexes in the presence of NTPs (lane 5), indicating that UvrD induces backtracking at multiple positions during elongation (Extended Data Fig. 2).

To determine whether the enzymatic activity of UvrD was required for the arrest, we repeated the above experiment with UvrD^{E221Q}; the E221Q mutation in the UvrD active site results in ∼600-fold decrease in helicase/translocase activity without significantly affecting binding of DNA, ATP[20] or RNAP (not shown). UvrD^{E221Q} failed to cause RNAP arrest during elongation (Fig. 1a, lanes 6, 7).

To confirm the requirement of ATP for UvrD-mediated transcriptional arrest, we walked RNAP to stalled elongation positions EC36–39, washed the beads to remove unincorporated NTPs and incubated the stalled complexes with UvrD ± ATP (Fig. 1b). After 1 min of incubation with UvrD + ATP most of EC36, EC38 and EC39 were inactivated: they failed to resume elongation upon addition of NTPs (lane 15); inactivation was almost complete after 2 min (lane 16). Without UvrD (lanes 2–6) or with UvrD lacking ATP (lanes 8–12), only ∼30% of EC39 was inactivated after 8 min of incubation, whereas EC36 and EC38 remained fully active. We conclude that UvrD induces RNAP backtracking at many positions through its ATP-dependent motor function (Extended Data Fig. 2).

To monitor the effect of UvrD on RNAP backtracking *in vivo*, we used a plasmid (p1EC) in which RNA synthesis initiated at a constitutive promoter is halted at a downstream position by the *lacO*-bound Lac repressor (Fig. 1c). The plasmid was designed so that the repressor blocked one isolated elongation complex[21]. Cells carrying pEC1 were transformed with a UvrD overexpression plasmid (pUvrD) or an empty vector (pVector). To monitor the effect of UvrD and the position of the halted elongation complex we performed *in situ* footprinting of its DNA bubble using the single-strand-specific probe, chloroacetaldehyde (CAA) (Fig. 1c). The halted elongation complex was clearly backtracked over a longer distance in the presence of pUvrD than empty vector: new CAA reactive sites were detected upstream and the reactivity of the downstream margin of the footprint was decreased (lane 4). Thus, as observed *in vitro*, UvrD also causes RNAP to backtrack *in vivo*.

UvrD facilitates NER by towing RNAP

RNAP stalled at DNA lesions presents a major obstacle for NER by obscuring damaged sites from repair enzymes[1]. The role of UvrD, therefore, could be to clear such lesions by forcing the obstructing elongation complex to backtrack. To test this hypothesis we reconstituted the first steps of NER *in vitro* (Fig. 2a and Extended Data Fig. 3). An initial elongation complex was assembled on DNA carrying a single cyclobutane pyrimidine dimer CPD) in the template strand at position +57 with respect to the transcriptional start site (Fig. 2a and Extended Data Fig. 3). CPD is the most common ultraviolet (UV)-induced lesion, a substrate for UvrABC and a roadblock for RNAP[22–24] (Extended Data Fig. 3). RNAP positioned 46 nucleotides upstream of CPD (EC11) did not affect UvrABC-directed CPD excision (Fig. 2a, lanes 3, 4, 7, 8). However, chasing EC11 to CPD inhibited the UvrC DNA cleavage reaction (lanes 11, 12). Addition of UvrD and ATP restored UvrC endonuclease activity at the CPD site (Fig. 2a, lanes 13–16), indicating that towing RNAP from the lesion site by UvrD is the first step of NER (Fig. 2a).

Anti-backtracking factors interfere with NER

In the RNAP 'towing' model of NER factors that normally inhibit backtracking may hinder the repair process: the GreA and GreB transcript cleavage factors[18] and active ribosomes control transcription elongation through this inhibition[21]. To test this prediction we used a primer extension assay to monitor UV-induced lesion repair *in vivo*. Such lesions block DNA polymerase, generating truncated primer extension products that can be analysed at single-nucleotide resolution[25]. We used a plasmid-borne *lacZ* gene isolated from wild-type and backtracking-prone *greA greB* mutant cells (Fig. 2b). The primer extension of *lacZ* DNA taken from both wild-type and mutant cells before and shortly after UV irradiation revealed truncated species unique to the irradiated DNA (Fig. 2b). However, the lesion repair rate (truncated species disappearance) was considerably higher in *gre⁻* cells than in wild-type cells. Only a few lesions were repaired at the same rate in wild-type and Gre-deficient cells. Because this assay detects any DNA damage that halts Taq DNA polymerase (not only pyrimidine dimers) we conclude that: (1) most UV-induced adducts within the transcribed region block the progression of RNAP, hampering the repair process, and (2) RNAP backtracking facilitates repair at most of damage sites.

If these conclusions are correct, GreA/GreB deficiency should suppress UvrD sensitivity to UV and genotoxic agents against which NER provides protection. We examined three genotoxic chemicals: mitomycin C, 4-nitroquinoline-1-oxide (4NQO) and cisplatin. These chemotherapeutics generate crosslinks and bulky DNA adducts that are predominantly processed by NER[26]. *uvrD* cells were highly sensitive to killing by all three agents, whereas inactivation of *greAB* greatly suppressed *uvrD* sensitivity to all three agents (Fig. 3a and Extended Data Fig. 4) and to UV irradiation (Fig. 3b and Extended Data Fig. 4c). As the function of GreAB is to suppress RNAP backtracking, we conclude that RNAP backtracking is required for efficient NER *in vivo* and that UvrD is responsible for much of the NER-associated RNAP backtracking during genotoxic stress.

In bacteria, active ribosomes control the rate of transcription elongation at protein coding sequences by 'pushing' RNAP forward[21], whereas inhibited ribosomes render cells highly resistant to UV-mediated lethality[27,28]. To test if active ribosomes interfere with NER by decreasing the frequency of backtracking we used a sublethal dose of chloramphenicol to slow ribosomes' translocation[21]. Analogous to the situation with Gre-deficiency, chloramphenicol rendered *uvrD* cells more resistant to 4NQO, mitomycin (Fig. 3a and Extended Data Fig. 4b) and UV (Fig. 3b and Extended Data Fig. 4d).

Collectively, these results argue that UvrD competes with anti-backtracking factors during genotoxic stress to promote NER (Fig. 3c). Interestingly, UvrD counteracts GreAB even under normal growth conditions, because *uvrD* inactivation suppresses the temperature sensitivity of *gre⁻* cells (Extended Data Fig. 5).

Mapping UvrD–elongation-complex interactions

We next mapped the location of UvrD within the elongation complex. Single-stranded/ duplex DNA junctions are the preferred UvrD loading sites[29]; therefore, the upstream exposed portion of the transcription bubble[30] is an optimal UvrD binding site. In this model, UvrD bound to RNAP pulls the elongation complex backwards while unwinding the upstream fork of the bubble (Fig. 3c). To locate UvrD within the elongation complex we incorporated photo-inducible 4[Author: 4′ (add prime symbol)?NO]-thio-deoxyuridine-5[Author: 5′ (add prime symbol)?YES]-monophosphate (sU[Author: is sU a standard nomenclature? NO what does the 's' stand for?Thio; you can use 4-thio-U instead]) into the non-template strand at different positions (relative to catalytic site) to induce protein–DNA crosslinks. The −1 and −9 sU probes generated major [Author: can you rephrase major? Do you mean abundant or the most abundant? most abundant]crosslinked species corresponding to ββ′ subunits of RNAP; their pattern didn't change in the presence of UvrD (Fig. 4a, lanes 5–8). A unique UvrD-specific crosslinked species was detected only with the −9 probe (lane 6) and was consistent with the UvrD adduct. No significant crosslinks were detected in front of RNAP (position +22). These results support [Author: the model?YES]that UvrD binds near the upstream fork of the transcription bubble.

To further map interactions between UvrD and the elongation complex, we used bis[sulfosuccinimidyl] suberate (BS3) to crosslink proximal lysine residues between UvrD and RNAP. Using mass spectrometry we identified three inter-protein crosslinks between UvrD and RNAP. These crosslinks mapped to ββ′ subunits of RNAP and clustered around the DNA binding region on UvrD (Fig. 4b and Extended Data Fig. 6). In particular, one crosslink, (β K909)–(UvrD K124), mapped to the β flap tip domain. During elongation, the flap tip is required for activity of the NusA elongation factor[31]. We propose that UvrD also binds RNAP proximal to the flap tip domain in a way that allows UvrD to reach the non-template DNA strand near the upstream fork of the bubble. The positions of the remaining two crosslinks (β′ K79)–(UvrD K389) and (β′ K40)–(UvrD K448) are consistent with this hypothesis (Fig. 4b and Extended Data Fig. 6).

Considering the proximity of UvrD and NusA [Author: perhaps as the start of a new paragraph define what you are referring to by 'their'?] on the surface of RNAP, and the fact

that NusA potentiates RNAP backtracking[32], we examined whether NusA supports UvrD-mediated backtracking. Indeed, NusA augmented UvrD-inducible arrests during elongation (Fig. 5a), providing a mechanistic explanation for the genetic evidence implicating NusA in Mfd-independent TCR[14]. Consistently, we showed that deletion of *greB* suppressed sensitivity of *nusA* cells (*nusA*[Author: should this and other symbols be italic?NO] and *nusA11*) to 4NQO, mitomycin C, nitrofurazone (NFZ) and UV (Fig. 5b and Extended Data Fig. 7). It has been reported that UvrD and NusA directly bind UvrB and UvrA, respectively[14,33,34]. Thus, not only do the two elongation factors act synergistically to clear RNAP from the lesion site, they probably also recruit UvrAB to the damage site to facilitate repair (Fig. 5c).

RNAP as a global DNA damage surveillance vehicle

A major challenge for NER is that UvrAB must recognize almost every type of bulky adduct on DNA among millions of normal base pairs in the genome. The aberrations detected by UvrAB range from apurinic/apyrimidinic (AP) sites to UV-induced photoproducts to large chemical adducts[2]. The accuracy and efficiency of the repair of such variable lesion types would be improved by a screening mechanism that recognizes a common structure or process, such as that of arrested RNAP during transcription elongation.

The preferential repair of the template DNA strand, that is, TCR, implies that the transcription apparatus augments the search and/or binding of lesions by NER enzymes[3]. Cellular RNAPs are highly sensitive to aberrations in the template strand, and are temporally or permanently blocked by various DNA adducts[22–24,35]. As bacterial and eukaryotic genomes are pervasively transcribed, RNAP can serve as a global surveyor of DNA damage that constantly monitors the quality of DNA via its natural one-dimensional diffusion. However, when stopped at DNA lesions, RNAP must either be terminated or moved aside to maintain damage site accessibility for NER. The Mfd pathway of TCR necessitates transcription termination[10], whereas the UvrD pathway described here uses RNAP backtracking. Importantly, this new UvrD mechanism facilitates NER without loss of RNAP, enabling transcription to promptly resume after DNA repair.

Mfd-independent TCR

The present work argues that the bulk of TCR occurs via UvrD-dependent backtracking (Fig. 5c); the sensitivity of *uvrD* and *nusA* cells to UV and various DNA damaging agents is much greater than that of *mfd* cells (Figs 3, 5b and Extended Data Figs 4, 7, 8). Yet, promoting backtracking by eliminating Gre factors, or by slowing ribosomal translocation, eliminates much of the DNA damage-induced lethality associated with UvrD or NusA deficiency (Figs 3, 5b and Extended Data Figs 4, 7). Consistently, deletion of DksA, a factor that competes with Gre for the secondary channel of RNAP, also increases *E. coli* sensitivity to mitomycin C[36]. Remarkably, deletion of *mfd* itself prominently suppresses *uvrD* sensitivity to UV and mitomycin C (Fig. 3b and Extended Data Figs 4, 8). This is consistent with the anti-backtracking mechanism of Mfd[8], further supporting the notion that RNAP backtracking is a prerequisite for the majority of [Author: can 'the majority of' be changed to 'most'?OK]NER events (Fig. 3d). Survival after genotoxic challenge depends on both

efficient NER and swift recovery from the SOS response. Indeed, *greAB* deletions facilitate NER, but do not increase cell survival (Fig. 3a, b). Similarly, Mfd function may not be as important for TCR per se, but instead for cellular recovery after the excessive backtracking associated with the SOS response.

In the absence of cellular stress, UvrD is equimolar with RNAP (∼3,000 molecules per cell[37]). During the SOS response, however, the intracellular level of UvrD increases approximately threefold[11]. This spike facilitates UvrD dimerization and helicase activity[38] and probably is a prerequisite for UvrD-mediated backtracking. A sigmoid-shaped graph of RNAP arrest as a function of UvrD concentration (Extended Data Fig. 9) supports this view. After washing, UvrD remains bound to RNAP (Extended Data Fig. 1b), yet loses backtracking ability (Fig. 1a), suggesting monomeric and multimeric associations with RNAP during periods of no stress and stress, respectively (Fig. 5c). Excessive backtracking can be detrimental to genomic integrity in cells recovering from genotoxic stress and resuming replication, as frequent co-directional collisions between the replisome and backtracked elongation complexes result in dsDNA breaks (DSBs)[39]. By 'pushing' backtracked RNAPs forward, Mfd suppresses DSBs associated with such collisions[39], and hence diminishes the high frequency of mutations associated with DSBs repair. This model is consistent with the reduced 'mutation frequency decline' phenotype of *mfd* cells as well as their high UV mutability, minimal UV sensitivity[40], and compromised transcriptional recovery after UV exposure[41].

The process of TCR and the basic structural organization of RNAPs are evolutionarily preserved[1,6,26]. Bulky DNA lesions, such as thymine dimers, stall bacterial and eukaryotic RNAPs similarly[22,23,42]. As backtracking is a fundamental feature of all RNAPs[17] and occurs pervasively throughout the eukaryotic genome[43], it is likely to drive TCR in higher organisms as well. Notably, mammalian [Author: human?]3′-5′ DNA helicase, XPB, and its homologs from other eukaryotes, associates with elongating RNAP II as a subunit of the TFIIH transcription factor. It has been implicated in NER as well as in several human disorders associated with deficient DNA repair[44,45]. It is thus possible that the mechanistic role of XPB is analogous to that described here for UvrD, that is, backtrack-inducing TCR.

Methods Summary

Cultures of *E. coli* were crosslinked with formaldehyde, collected by centrifugation, and lysed. RNAP-containing material was pulled down with anti-RNAP antibodies and proteins were identified by mass spectrometry. For DNA damage experiments, colony-forming units were counted after exposure to increasing concentrations of 4-NQO, mitomycin C or cisplatin. For UV survival assays, diluted cultures were plated, irradiated with a UV lamp, and incubated overnight in the dark. Strains were transformed with pUC18 plasmid and induced with IPTG before and after irradiation. *In vitro* transcription assays were performed as described[16]. RNA-DNA scaffolds containing cyclo-thymine dimers or 4-thio-dUMP-modified template oligonucleotides were assembled with immobilized, biotinylated RNAP before incubation with components of UvrABC system or irradiation at 308 nM for protein–DNA crosslinking, respectively. Purified RNAP and UvrD were crosslinked with BS3, and crosslinked proteins were reduced with dithiothreitol (DTT), alkylated with iodoacetamide

and digested with trypsin. Tryptic peptides were analysed with a mass spectrometer coupled to a liquid chromatography system. pLink[46] was used to search Mascot generic format files for inter-peptide crosslinks. For *in situ* DNA footprinting, the *uvrD* gene was cloned into a vector under the $P_{LtetO-1}$ promoter, and induced with anhydrotetracycline for 1 h before CAA modification. CAA modifications on non-template DNA were analysed with primer extension using [^{32}P]-labelled primer in parallel with the sequencing reactions.

Methods

Bacterial strains

The strains used in this study are listed in Extended Data Table 1 and were constructed using standard genetic techniques.

Mass spectrometry of *in vivo* RNAP interactome

Mid-exponential cultures of *E. coli* K12 MG1655 were treated with formaldehyde (Thermo Fisher, final concentration 50 mM) for 30 min, cells were collected by centrifugation, and lysed by a combination of ultrasound disruption and the action of lysozyme (human recombinant, Sigma-Aldrich). Pull-down of RNAP-containing material was performed using a mix of anti-RNAP antibodies (Neoclone) immobilized on Protein A/G Mag Sepharose beads (GE). Protein identification in the pull-down material was carried out at the NYUMC Protein Core Mass Spectrometry Facility, using an LTQ-Orbitrap mass spectrometer followed by Mascot database search (Matrixscience). Protein abundance was estimated using emPAI scores[15]. The range of emPAI values for a representative set of proteins in RNAP pull-downs spans 3 independent experiments (Extended Data Fig. 1).

Measuring sensitivity to DNA damage

E. coli strains were cultured in LB medium overnight. Appropriate dilutions were spread on LB agar plates containing increasing concentrations of 4-NQO or NFZ or mitomycin C or cisplatin, followed by an overnight incubation at permissive temperatures. Colony-forming units (c.f.u.) were counted at each concentration of genotoxic agents. Chloramphenicol was used at the sublethal concentration (1.0 μg ml^{-1}), along with genotoxic agents. A 10 mM stock solution of NFZ or 4-NQO was first made in *N,N*-dimethylformamide, stored at −20 °C, and diluted appropriately for each experiment. Mitomycin C was dissolved in sterile saline to a concentration of 500 μg ml^{-1} and stored at −20 °C. Cisplatin was dissolved in LB medium to a concentration of 500 μg ml^{-1} just before use. For UV survival assays, overnight grown cultures were diluted in M9 minimal salts, appropriate dilutions were spread on LB agar plates and irradiated with a UV (254 nm) lamp and incubated overnight in the dark at appropriate temperatures.

In vivo TCR

Strains MG1655Z1 and MG1655Z1 *greA greB* were transformed with pUC18 plasmid. Overnight cultures were diluted 1:100 in LB medium supplemented with 100 μg ml^{-1} ampicillin and grown until OD$_{600}$ ∼0.3 at 30 °C. The culture was centrifuged at 5000 rpm for 5 min. The pellet was resuspended in M56 to an absorbance of 0.4.

The resuspended culture was spread on a Petri dish and, whilst being shaken, irradiated with 70 J per m^2 of 254 nm UV light. To induce the transcription on pUC18, 1 mM isopropyl-β-ᴅ-thiogalactoside (IPTG) was added to the culture medium 1 h before and immediately after UV irradiation. The irradiated culture was then supplemented with 0.25% casamino acids, 0.004% thiamine and 0.4% glucose and incubated at 30 °C in the dark to avoid removal of cyclobutane dimers by photoreactivation. Cells were collected before UV irradiation (-), immediately after (time 0 repair) and at defined repair times (15, 30, 45 and 60 min). Plasmid DNA was isolated from the cultures using a Qiagen plasmid isolation kit.

Primer extension was performed with (^{32}P)-labelled primers for analysis of cyclobutane pyrimidine dimers on the template strand. End labelled primer, 50 pmol, (5′-GGCATGCAAGCTTGGCACTGGC-3′), 400 μM dNTPs, 200 ng of plasmid DNA and *Taq* DNA polymerase were mixed in Thermopol buffer. The mixture was denatured by heating to 98 °C in a thermal cycler for 5 min followed by annealing at 55 °C for 5 min. Primer extension was performed at 68 °C for 6 min. Formamide stop solution was added to the reaction mixture and aliquots loaded onto a 6% urea-polyacrylamide gel. Percentages of repaired DNA were calculated using Image-Quant (GE) and averaged from three independent experiments with untreated samples taken as 100%.

In vitro transcription assays

E. coli RNAP and UvrD were purified as described in refs 16 and 48, respectively. DNA templates were constructed using the non-transcribed part of T7 A1 promoter fragments fused to appropriate transcription units. Resulting DNA fragments were PCR amplified and purified from an agarose gel. For biotinylated DNA templates, biotinylated DNA oligonucleotides (IDT) were used. All NTP substrates were purified by ion-exchange chromatography[16]. Transcription at the T7A1-promoter templates was initiated by mixing 1 pmol of RNAP with equimolar amount of appropriate DNA PCR fragments in TB50 buffer (40 mM Tris-HCl pH 8.0; 10 mM $MgCl_2$; 50 mM NaCl) followed by addition of 10 μM ApUpC RNA primer, 25 μM ATP and GTP. Incubation was continued for 5 min at 37 °C. Resulting complexes were labelled by addition of 2 μCu α-[^{32}P]-CTP (3,000 Ci mmol^{-1}; MP Biomedicals) for 5 min at room temperature and immobilized on Neutravidin beads (5–10 μl; Piers) in the presence of 1.5 mg ml^{-1} heparin. The resulting EC20 was washed twice with 1 ml of TB1000 (TB with 1 M NaCl), twice with 1 ml of TB100 and divided into 10 μl aliquots. For the chase experiments, the EC20 was incubated with either the indicated amounts of UvrD or equal volumes of mock buffer for 5 min at room temperature and then chased for 5 min at 37 °C by addition of 0.1 mM NTPs. Where indicated, beads were washed after the chase with 1 ml of TB1000 and 1 ml of TB100. All reactions were stopped by equal volume of Stop Buffer (SB, 1×TBE buffer, 8 M Urea, 20 mM EDTA, 0.025% xylene cyanol, 0.025% bromophenol blue). For the GreB cleavage assay (Fig. 2a), two 10 μl aliquots were incubated for 5 min at room temperature with 1 μM GreB. One aliquot was then chased for 5 min by addition of 0.1 mM NTPs and both samples were quenched as above. To test the effect of NusA on UvrD-induced backtracking (Fig. 5a), the initial EC20 was prepared as above and incubated with the indicated amounts of UvrD in the absence or presence of 10 nM NusA. Reaction mixtures were chased as above. For the UvrD-induced formation of stalled ECs (Fig. 2b), EC20 was walked to position 36–39 as described in ref.

16. The resulting ECs were mixed with 12.5 nM UvrD and 1 mM ATP or an equal amount of mock solution and incubated at 37 °C for the indicated time intervals. Next, 10 μl aliquots were withdrawn and mixed with 0.1 mM GTP and CTP for 5 min at room temperature. Reactions were stopped by addition of equal volumes of SB. The amount of UvrABC-mediated DNA cleavage products after 30 min at 37 °C was taken as 100% and UvrABC-mediated cleavage after CTP + GTP chase was calculated as a fraction of that value. Image-Quant (GE) software was used for all quantifications.

Reconstitution of the EC and UvrABC-mediated processing of thymine dimers

For assembly of the RNA-DNA scaffold (Fig. 2a), 75 pmol A1 RNA (IDT) were mixed with 75 pmol of the cyclo-thymine dimer template DNA strand or control strand (Midland, TX) in 20 μl of the annealing buffer (AB) (12% glycerol; 20 mM Tris pH 8.0; 40 mM KCl; 5 mM MgCl$_2$) and annealed gradually in a PCR cycler. The resulting scaffold was stored at −20°C and used as needed. To measure the extent of UvrABC-directed cleavage, 15 pmol of the DNA–RNA scaffold were mixed with 15 pmol of biotinylated RNAP in 20 μl of AB and incubated for 10 min at room temperature. 75 pmol of non-template strand was added and incubation continued for another 5 min. The resulting complex was immobilized at Neutravidin-coated beads (Pierce), washed twice with TB1000 and then with TB100. For RNA labelling, 5 μM ATP and 2 μCu α-[^{32}P]-CTP were added for 5 min at room temperature, followed by washing with TB100. For the UvrC cleavage reaction complexes were washed twice with TB0 (20 mM Tris-HCl pH 8.0; 10 mM MgCl$_2$) and 10× PNK buffer (New England Biolabs) was added together with 1 μCu γ-[^{32}P]-ATP (7,000 Ci mmol^{-1}; MP Biomedicals) and 20 units PNK (New England Biolabs). The DNA labelling reaction continued for 30 min at 37 °C, then the beads (EC11) were washed twice with TB1000 and TB100. EC11 were processed directly or chased first for 10 min at 37 °C by the addition of 1 mM NTPs. Complexes were supplemented with 1 mM ATP and 12.5 nM UvrD was added where indicated for 10 min at 37 °C before washing with TB100. To initiate the cleavage reaction premixed UvrA (2.5 nM), UvrB (10 nM) and UvrC (25 nM) were added and incubated for the indicated time intervals at 37 °C before quenching with SB. UvrABC were purified as described in ref. 49. Products of all reactions were separated in 6–23% denaturing polyacrylamide gels and visualized via phosphor-imaging using a Typhoon phosphor-imager (GE Healthcare) and Image Quant software (GE Healthcare).

Protein–DNA crosslinking

RNA–DNA scaffolds were assembled as above using the 4-thio-dUMP-modified template oligos (Midland, TX), A1 RNA (9 nt long), and non-template DNA. Resulting complexes were labelled as described above and incubated with 12.5 nM UvrD or mock solution for 5 min at 37 °C before being irradiated for 10 min with a hand-held UV lamp (Cole Parmer) at 308 nM wavelength. Irradiation was performed on ice and samples were denatured in Laemmli loading buffer. Products were separated in a 6% denaturing polyacrylamide gel with 0.1% SDS and Tris-glycine running buffer. UvrD adducts were seen on the gel as a 90 kDa species.

UvrD-RNAP binding assay

UvrD and RNAP, UvrD alone, and RNAP alone were incubated at room temperature for 30 min in binding buffer (50 mM Tris pH 8.0, 100 mM NaCl, 50 mM imidazole) before they were added to His Mag Sepharose Ni beads (GE), which were pre-equilibrated and washed with binding buffer. Each was then incubated for 30 min with gentle agitation at room temperature. After incubation, beads were washed three times with binding buffer and eluted in 50 μl of elution buffer (50 mM Tris pH 8.0, 100 mM NaCl, 400 mM imidazole). Samples were electrophoresed in an SDS-polyacrylamide gel alongside pure UvrD, for reference.

RNAP-UvrD cross-linking and their mapping by LC-MS/MS

Purified RNAP at a final concentration of 2 μM was incubated with 4 μM UvrD in crosslinking buffer (1× PBS, 500 mM NaCl, pH 7.4) for 30 min at room temperature. Crosslinking was initiated upon addition of Bis(sulfosuccinimidyl) suberate (BS3) (Thermo Scientific) in 1×PBS at a final concentration of 350 μM. Crosslinking reactions continued for 30 min at room temperature before they were quenched with 1 M Tris pH 8.0 at a final concentration of 200 mM.

Crosslinked proteins were separated by SDS–PAGE (4–12% Bis Tris Novex gels, Invitrogen) and stained with GelCode Blue. Super-shifted (relative to positions of untreated RNAP subunits) were removed from the gel and destained. Samples were reduced with 20 mM DTT (Sigma) at 57 °C for 60 min and alkylated with 45 mM iodoacetamide (Sigma) in the dark for 45 min at room temperature before overnight, in-gel digestion with 0.5 μg sequencing grade modified trypsin (Promega).

Gel slices were incubated with Poros R2 50 μm slurry diluted in 5% formic acid and 0.2% TFA to bind tryptic peptides. The Poros bead slurry was collected and washed through C18 Zip Tips (Millipore) before elution with 40 μl of 40% acetonitrile in 0.5% acetic acid. Eluted peptides were dehydrated in vacuum and resuspended in 40 μl 0.5% acetic acid for MS analysis.

Peptide aliquots (∼200 ng) were analysed in the Q Exactive mass spectrometer (Thermo Scientific) coupled to an EASY-nLC (Thermo Scientific) liquid chromatography system. The peptides were eluted over a 120-min linear gradient from 98% buffer A (water) to 40% buffer B (ACN) then continue to 100% buffer B over 10 min with a flow range of 200 nl min^{-1}. Each full MS scan (R = 70,000) was followed by dd-MS^2 (R = 17,500) with HCD and an isolation window of 2.0 *m/z*. Normalized collision energy was set to 35. Precursors of +1, +2 and +3 were excluded from MS2 scans; monoisotopic screening was enabled and a dynamic exclusion window was set to 30.0 s.

Identification of cross-links: Mascot generic format (mgf) files were generated from Xcalibur raw files using the Proteome Discoverer software (Thermo Scientific). pLink[46] was used to search resulting mgf files for interpeptide crosslinks with the following settings: precursor mass tolerance 20 p.p.m.; fragment mass tolerance 5 p.p.m.; BS3 crosslinker (crosslink monoisotopic mass shift of 138.0680786 Da, monolink mass shift of 156.0786442 Da. One fixed modification (Carbamidomethyl-C) and three variable modifications (oxidation-M, N-terminal glutamate to pyroglutamate, N-terminal acetylation) were

specified. False discovery rate was set at <5%. Fragmentation spectra for each crosslinked peptide were validated using pLabel[50] and confirmed with manual inspection.

In situ DNA footprinting

To construct the plasmid pUvrD (Cm^r, p15a), the *uvrD* gene was excised from the plasmid pETDuet-uvrD as an XhoI / filled-in XbaI fragment and cloned into the pZA31 vector at the SalI site (compatible cohesive end with XhoI) and the blunted KpnI site. The expression of the *uvrD* gene in the resulting plasmid is driven by the P_L-derivative promoter $P_{LtetO-1}$ which is controlled by the operator repressor system of the Tn*10*-derived *tet* resistance operon[51]. The induction of $P_{LtetO-1}$ is achieved by anhydrotetracycline.

To ensure expression of the regulatory repressor proteins LacI and TetR, the entire unit encoding *Lac*R, *Tet*R and Sp^{r53} was transferred into the chromosome of *E. coli* strain MG1655 by P1 transduction (MG1655Z1).

E. coli strains were grown in 10 ml of M9 medium supplemented with 0.4% glucose, 4 mg ml^{-1} casamino acids, 100 μg ml^{-1} ampicillin and 30 μg ml^{-1} chloramphenicol. To induce the $P_{LtetO-1}$ promoter, anhydrotetracycline (50 ng ml^{-1}) was added for 1 h before CAA modification. At OD_{600}~0.6 1 mM IPTG was added (if required) for 10 min, then CAA was added to 4% final concentration and the incubation was continued for 7 min. Then cells were collected, immediately washed with the saline solution, collected and the plasmid DNA extracted.

To analyse CAA modification[52] of the non-template DNA strand, primer extension was performed with [^{32}P]-labelled primer (5′-TAGCTTCCTTAGCTCCTGA-3′) in parallel with the sequencing reactions in a cycler at the following conditions: 94 °C for 3 min (initial denaturation), then 94 °C for 30 s (denaturation), 56 °C for 30 s (annealing), 72 °C for 60 s (extension), 25 cycles total. Formamide stop solution was added to the reaction mixture and aliquots were analysed by electrophoresis in an 8% urea-polyacrylamide gel.
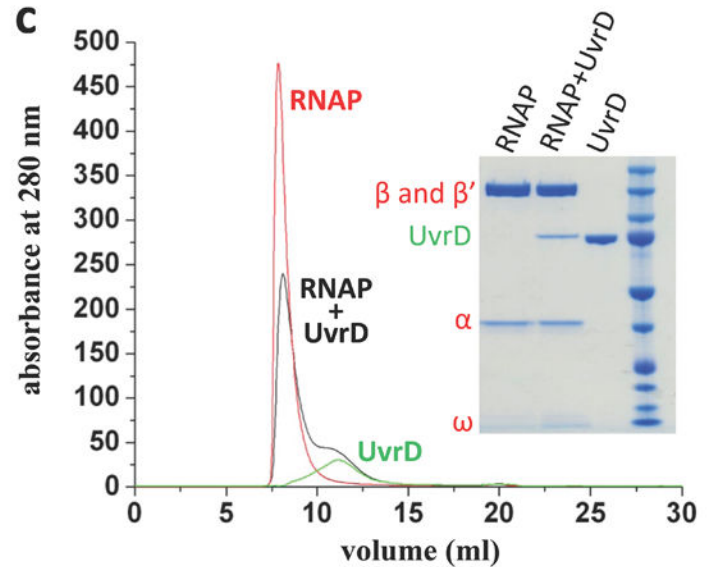
Extended Data

a

PROTEIN NAME	emPAI RANGE
RNA polymerase	
RpoC	5.67 - 19.21
RpoB	4.34 - 15.73
RpoA	2.37 - 9.43
RpoZ	2.22 - 4.13
Transcription factors	
RpoD	1.35 - 7.97
NusG	0.58 - 2.25
Rho	0.15 - 2.25
NusA	0.06 - 1.26
CAP	0.09 - 0.30
DNA repair	
UvrD	0.51 – 1.11
UvrA	0.09 – 0.70
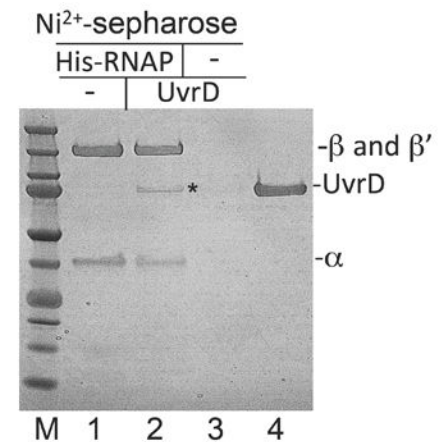
Extended Data Figure 1. UvrD binds RNAP

a, A sample list of RNAP-bound proteins from exponentially grown *E. coli*. Abundance is based on emPAI score[15]. **b**, UvrD + 6His–RNAP, UvrD, or 6His–RNAP were affinity-purified on nickel beads and electrophoresed alongside pure UvrD, for reference; The asterisk indicates UvrD. **c**, RNAP-UvrD complex isolated by size-exclusion chromatography. UvrD–RNAP were mixed 3:1, and run over a Superdex 200 10/300GL column. RNAP core (red) and UvrD (green) chromatograms are overlaid for comparison. The inlaid polyacrylamide gel displays fractions taken from each chromatographic peak.
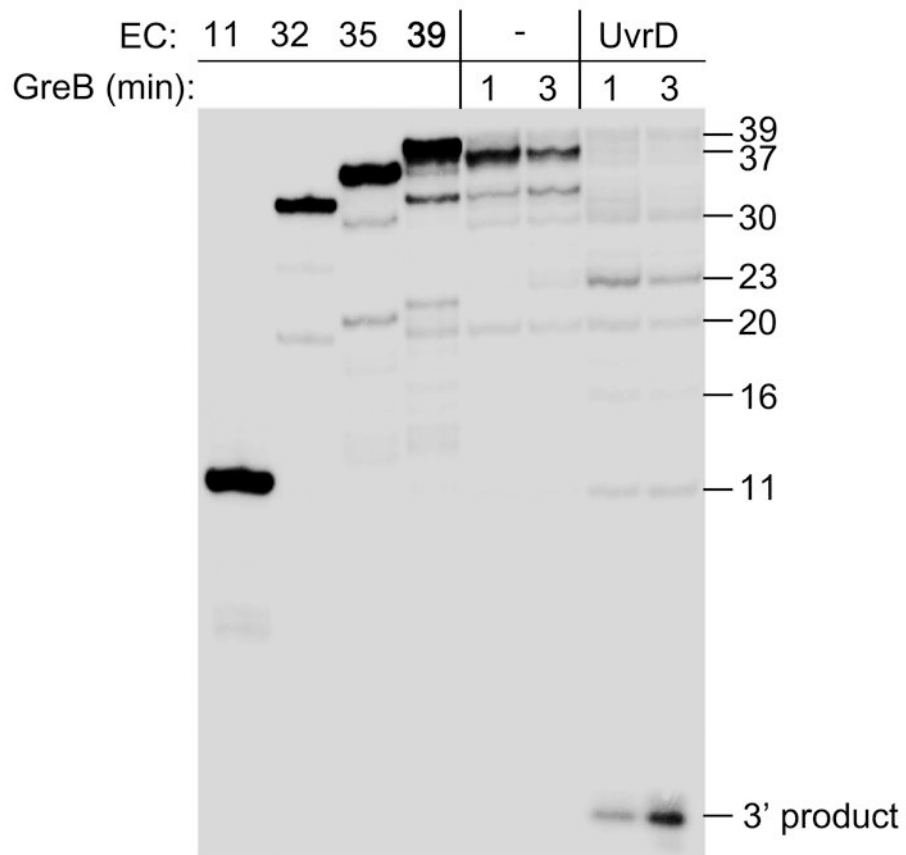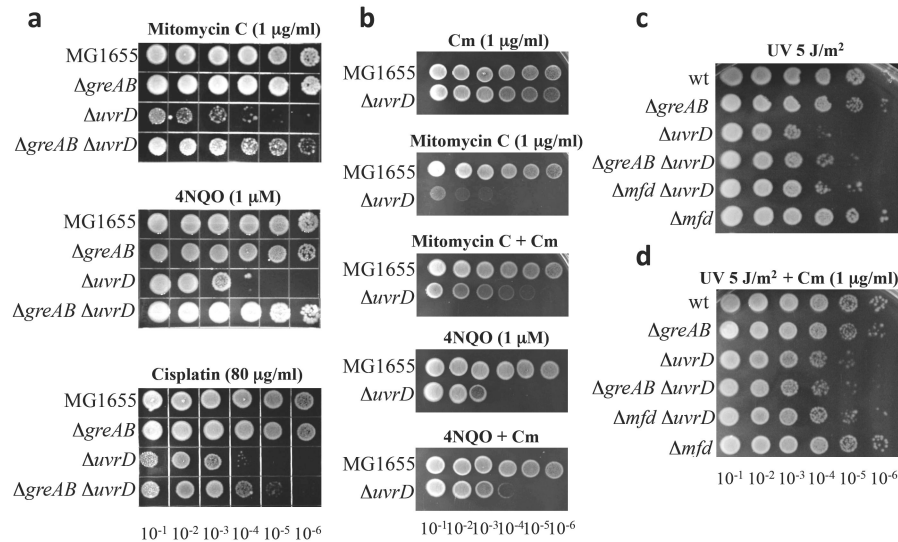
Extended Data Figure 2. UvrD promotes long-range backtracking

Biotinylated RNAP was used to prepare the startup EC11 immobilizing on beads. It was walked to position 39, followed by incubation with UvrD, washing (to remove UvrD and NTPs), and then treatment with GreB for indicated times. Numbers on the right indicate the size of 5′-labelled RNAs.
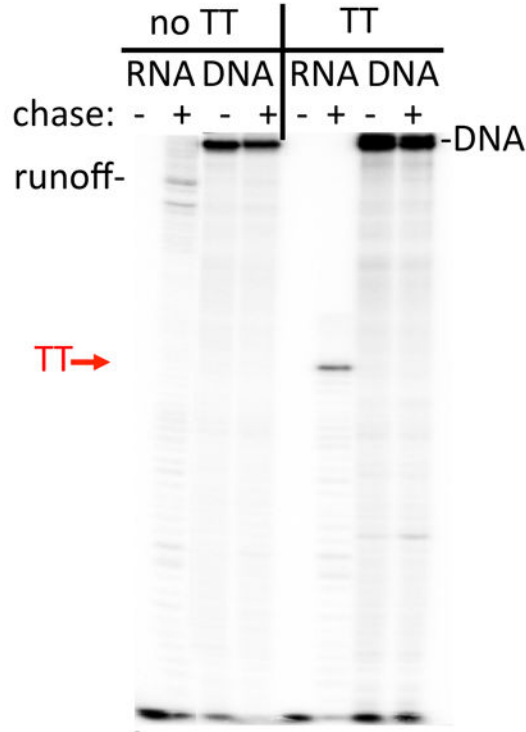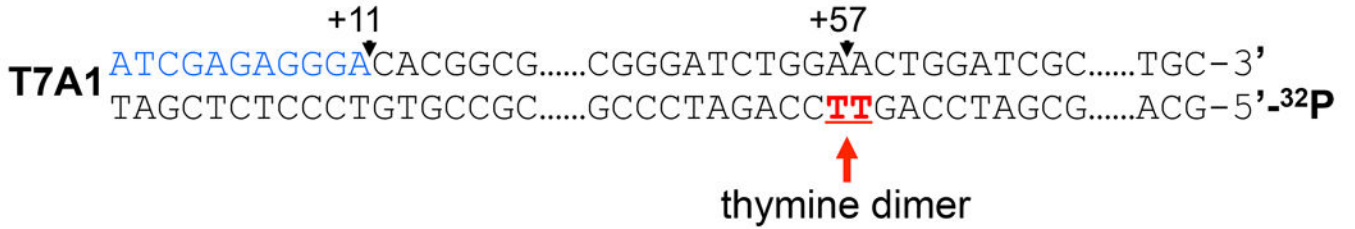
Extended Data Figure 3. Thymine dimer in the template strand blocks the elongation complex
Schematic diagram of the T7A1 promoter template shows the position of CPD (red). Both control (no TT) and CPD-bearing template strands were radiolabelled at their 5′ ends (top band). The sequencing gel also shows the radiolabelled RNA products before and after chase of EC11. The EC was completely halted by CPD (indicated by red TT). On the control template it formed the runoff products.

a Mitomycin C (1 μg/ml)

MG1655
ΔgreAB
ΔuvrD
ΔgreAB ΔuvrD

4NQO (1 μM)

MG1655
ΔgreAB
ΔuvrD
ΔgreAB ΔuvrD

Cisplatin (80 μg/ml)

MG1655
ΔgreAB
ΔuvrD
ΔgreAB ΔuvrD

10^{-1} 10^{-2} 10^{-3} 10^{-4} 10^{-5} 10^{-6}

b Cm (1 μg/ml)

MG1655
ΔuvrD

Mitomycin C (1 μg/ml)

MG1655
ΔuvrD

Mitomycin C + Cm

MG1655
ΔuvrD

4NQO (1 μM)

MG1655
ΔuvrD

4NQO + Cm

MG1655
ΔuvrD

10^{-1} 10^{-2} 10^{-3} 10^{-4} 10^{-5} 10^{-6}

c UV 5 J/m²

wt
ΔgreAB
ΔuvrD
ΔgreAB ΔuvrD
Δmfd ΔuvrD
Δmfd

d UV 5 J/m² + Cm (1 μg/ml)

wt
ΔgreAB
ΔuvrD
ΔgreAB ΔuvrD
Δmfd ΔuvrD
Δmfd

10^{-1} 10^{-2} 10^{-3} 10^{-4} 10^{-5} 10^{-6}

Extended Data Figure 4. Effect of *greAB, mfd* and ribosome inactivation on *uvrD* sensitivity to DNA damaging agents and UV

a, Representative efficiencies of colony formation of wild-type (MG1655) and mutant *E. coli* cells in the presence of the indicated amounts of mitomycin C, 4NQO and cisplatin. Cells were spotted on LB agar plates in serial tenfold dilutions and incubated at 30 °C for 24 h. **b**, Representative efficiencies of colony formation of wild-type and uvrD cells in the presence of the indicated amounts of mitomycin, 4NQO and chloramphenicol. Cells were spotted on LB agar plates in serial tenfold dilutions and incubated at 30 °C for 24 h. **c**, Representative efficiencies of colony formation of wild-type (MG1655) and mutant *E. coli* cells after UV irradiation. Cells were spotted on LB agar plates in serial tenfold dilutions and incubated at 30 °C for 24 h. **d**, Representative efficiencies of colony formation of wild-type and mutant *E. coli* cells after UV irradiation in the presence of a sublethal dose of chloramphenicol. Cells were spotted on LB agar plates in serial tenfold dilutions and incubated at 30 °C for 24 h.

A - MG1655
B - ΔuvrD
C - ΔgreA ΔgreB
D - ΔgreA ΔgreB ΔuvrD

30° C   37° C   42° C
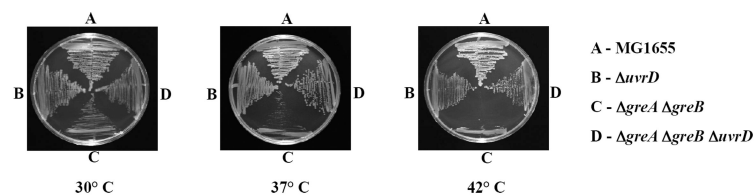
Extended Data Figure 5. UvrD inactivation suppresses temperature sensitivity of *greAB* cells
E. coli strains were streaked on LB agar plates and incubated at the indicated temperatures for 24 h.
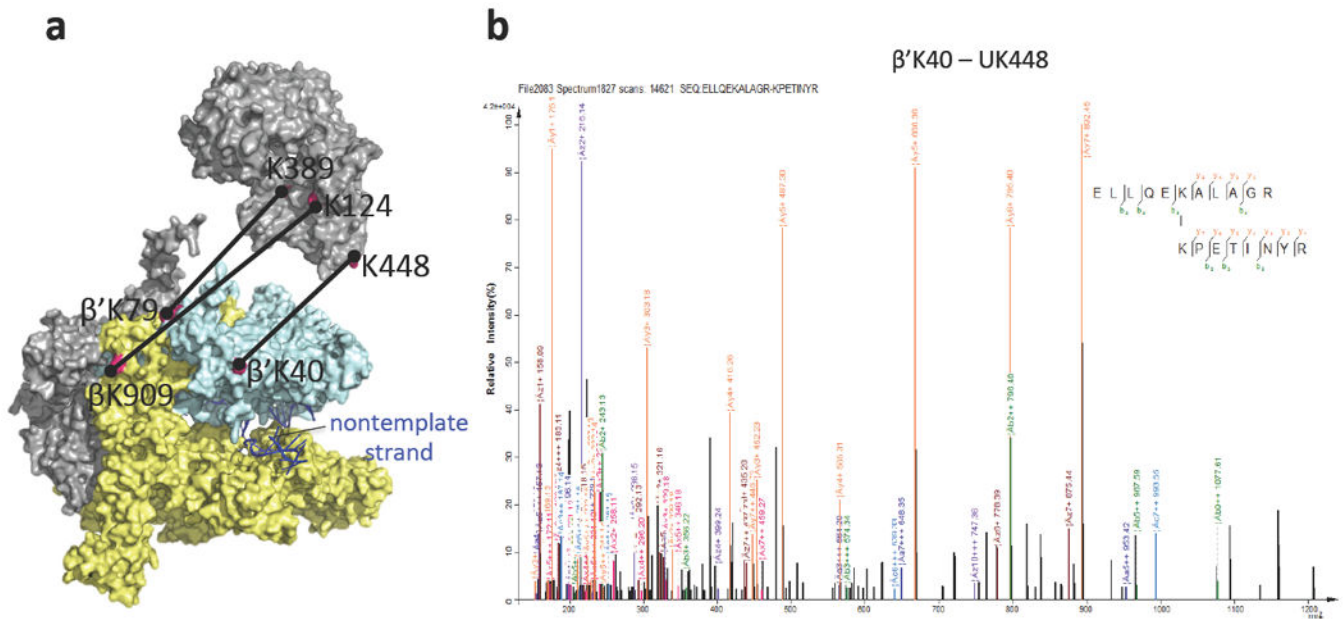
Extended Data Figure 6. UvrD–RNAP crosslinks

a, Three inter-protein crosslinks indicate that UvrD binds near the β flap on RNAP. UvrD (grey, PDB accession code 2IS4) cross-links to RNAP (PDB accession code 4IGC) at three distinct positions that span the β (pale yellow) and β′ (light blue) subunits of RNAP. The non-template strand (blue, PDB accession code 4G7O) is indicated for reference. Crosslinked lysines are colored magenta and pairs are connected with a black line. **b**, MS2 spectrum of a representative crosslinked pair (β′ K40)–(UvrD K448). The peptide sequences with cross-linked lysine residues are shown (top right). Observed peptide backbone cleavage is indicated and b- and y-type fragment ions are labelled in the spectrum. The *m/z* tolerances of fragment ions are presented in the inset below the spectra. Spectra were annotated using pLabel[50].
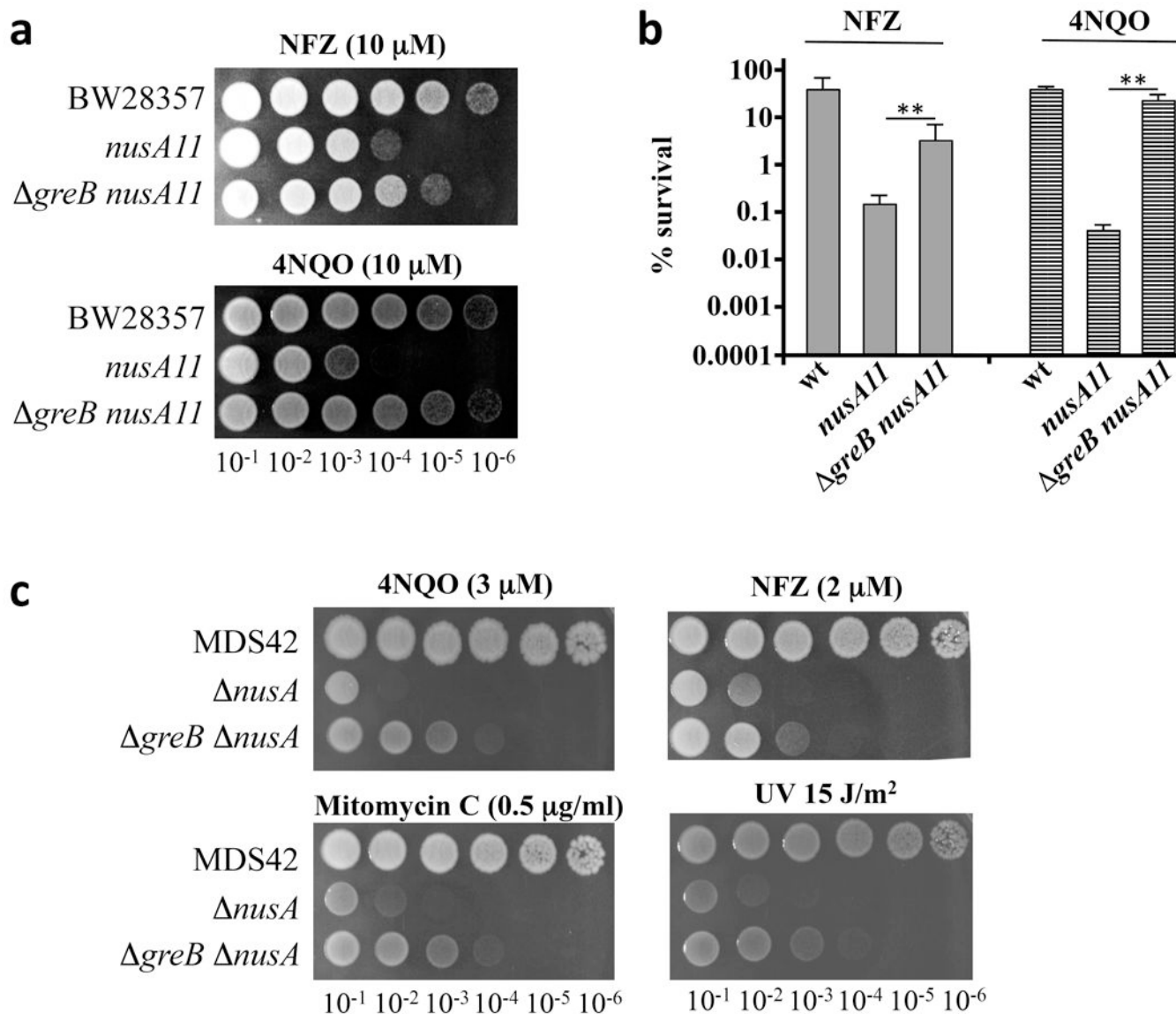
Extended Data Figure 7. GreB inactivation suppresses *nusA* sensitivity to genotoxic chemicals and UV

a, Representative efficiencies of colony formation of wild-type (MG1655) and mutant *E. coli* cells in the presence of indicated amounts of NFZ and 4NQO. Cells were spotted on LB agar plates in serial tenfold dilutions and incubated at 30 °C for 24 h. **b**, Data from three independent experiments are presented as the mean ± s.e.m.; **$P < 0.01$. **c**, Representative efficiencies of colony formation of MDS42 and mutant *E. coli* cells in the presence of indicated amounts of mitomycin, 4NQO, NFZ and after UV irradiation. Cells were spotted on LB agar plates in serial tenfold dilutions and incubated at 30 °C for 24 h.
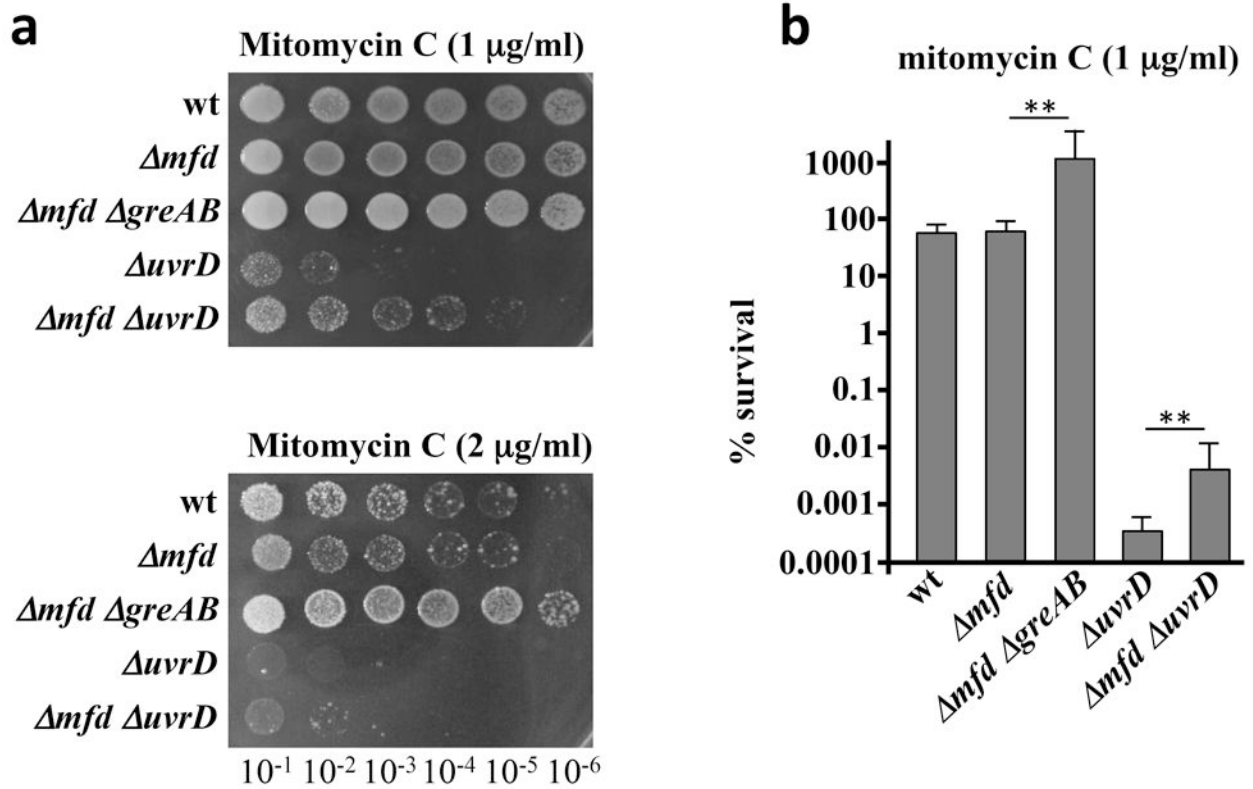
Extended Data Figure 8. Deletion of *mfd* partially suppresses *uvrD* sensitivity to mitomycin C
a, Representative efficiencies of colony formation of wild-type (MG1655) and mutant *E. coli* cells in the presence of indicated amounts of mitomycin C. Cells were spotted on LB agar plates in serial tenfold dilutions and incubated at 30 °C for 24 h. **b**, Data from three independent experiments are presented as the mean ±s.e.m.; **P < 0.01.
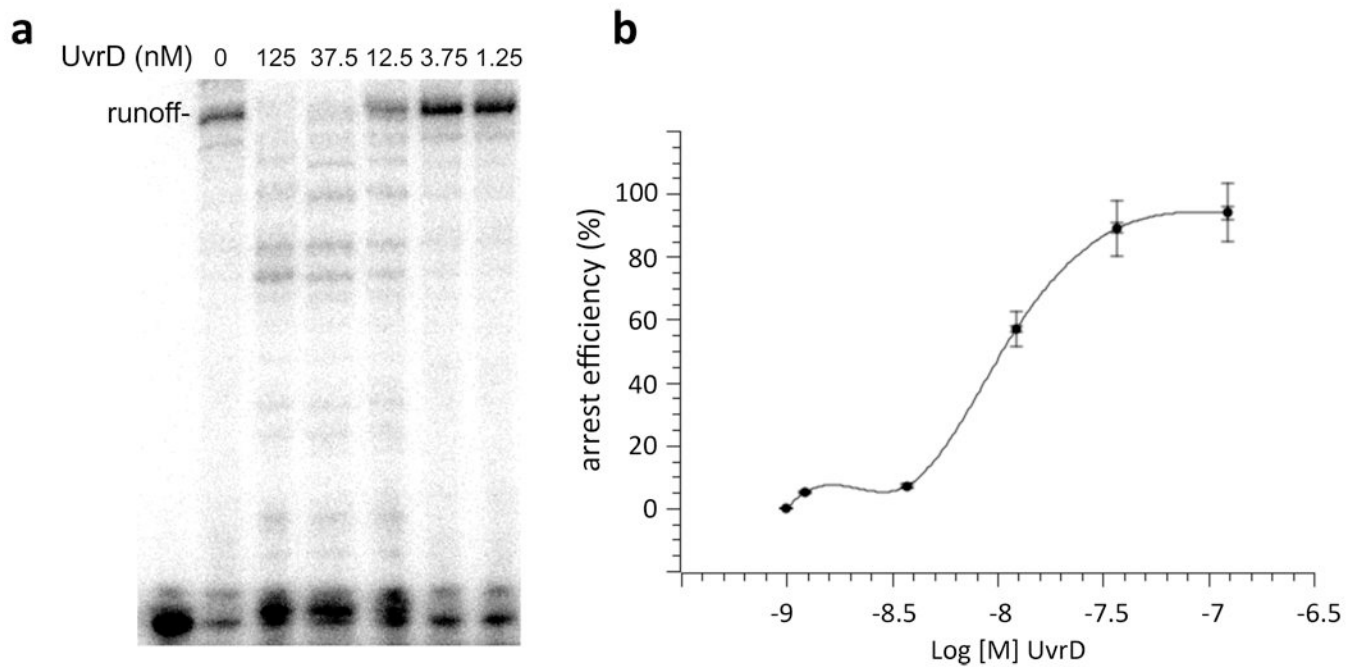
Extended Data Figure 9. Transcriptional arrest as a function of UvrD concentration
a, A representative chase experiment demonstrating multiple transcriptional arrests as a function of UvrD concentration. **b**, Data from three independent experiments are plotted as the mean ± s.e.m. Arrest efficiency (%) was calculated as a fraction of all arrested complexes in relation to the full-length runoff.

Extended Data Table 1 *Escherichia coli* strains used in this study.

Acknowledgments

References

1. Reardon JT, Sancar A. Nucleotide excision repair. Prog Nucleic Acid Res Mol Biol. 2005; 79:183–235. Medline CrossRef. [PubMed: 16096029]

2. Van Houxen B, McCullough A. Nucleotide excision repair in *E. coli*. Ann NY Acad Sci. 1994; 726:236–251. Medline CrossRef. [PubMed: 8092680]

3. Ganesan A, Spivak G, Hanawalt PC. Transcription-coupled DNA repair in prokaryotes. Prog Mol Biol Transl Sci. 2012; 110:25–40. Medline CrossRef. [PubMed: 22749141]

4. Truglio JJ, Croteau DL, Van Houten B, Kisker C. Prokaryotic nucleotide excision repair: the UvrABC system. Chem Rev. 2006; 106:233–252. Medline CrossRef. [PubMed: 16464004]

5. Mellon I, Hanawalt PC. Induction of the *Escherichia coli* lactose operon selectively increases repair of its transcribed DNA strand. Nature. 1989; 342:95–98. Medline CrossRef. [PubMed: 2554145]

6. Gaillard H, Aguilera A. Transcription coupled repair at the interface between transcription elongation and mRNP biogenesis. Biochim Biophys Acta. 2013; 1829:141–150. Medline CrossRef. [PubMed: 23046879]

7. Deaconescu AM, et al. Structural basis for bacterial transcription-coupled DNA repair. Cell. 2006; 124:507–520. Medline CrossRef. [PubMed: 16469698]

8. Park JS, Marr MT, Roberts JW. *E. coli* Transcription repair coupling factor (Mfd protein) rescues arrested complexes by promoting forward translocation. Cell. 2002; 109:757–767. Medline CrossRef. [PubMed: 12086674]

9. Savery N. Prioritizing the repair of DNA damage that is encountered by RNA polymerase. Transcription. 2011; 2:168–172. Medline CrossRef. [PubMed: 21922058]

10. Selby CP, Sancar A. Molecular mechanism of transcription-repair coupling. Science. 1993; 260:53–58. Medline CrossRef. [PubMed: 8465200]

11. Kumura K, Sekiguchi M. Identification of the *uvrD* gene product of *Escherichia coli* as DNA helicase II and its induction by DNA-damaging agents. J Biol Chem. 1984; 259:1560–1565. Medline. [PubMed: 6319401]

12. Lee JY, Yang W. UvrD helicase unwinds DNA one base pair at a time by a two-part power stroke. Cell. 2006; 127:1349–1360. Medline CrossRef. [PubMed: 17190599]

13. Matson SW, George JW. DNA of helicase II *Escherichia coli*. Characterization of the single-stranded DNA-dependent NTPase and helicase activities. J Biol Chem. 1987; 262:2066–2076. Medline. [PubMed: 3029063]

14. Cohen SE, et al. Roles for the transcription elongation factor NusA in both DNA repair and damage tolerance pathways in *Escherichia coli*. Proc Natl Acad Sci USA. 2010; 107:15517–15522. Medline CrossRef. [PubMed: 20696893]

15. Ishihama Y, et al. Exponentially modified protein abundance index (emPAI) for estimation of absolute protein amount in proteomics by the number of sequenced peptides per protein. Mol Cell Proteomics. 2005; 4:1265–1272. Medline CrossRef. [PubMed: 15958392]

16. Nudler E, Gusarov I, Bar-Nahum G. Methods of walking with the RNA polymerase. Methods Enzymol. 2003; 371:160–169. Medline CrossRef. [PubMed: 14712698]

17. Nudler E. RNA polymerase backtracking in gene regulation and genome instability. Cell. 2012; 149:1438–1445. Medline CrossRef. [PubMed: 22726433]

18. Borukhov S, Sagitov V, Goldfarb A. Transcript cleavage factors from *E. coli*. Cell. 1993; 72:459–466. Medline CrossRef. [PubMed: 8431948]

19. Nudler E, Mustaev A, Lukhtanov E, Goldfarb A. The RNA-DNA hybrid maintains the register of transcription by preventing backtracking of RNA polymerase. Cell. 1997; 89:33–41. Medline CrossRef. [PubMed: 9094712]

20. Brosh RM Jr, Matson SW. Mutations in motif II of *Escherichia coli* DNA helicase II render the enzyme nonfunctional in both mismatch repair and excision repair with differential effects on the unwinding reaction. J Bacteriol. 1995; 177:5612–5621. Medline. [PubMed: 7559350]

21. Proshkin S, Rahmouni AR, Mironov A, Nudler E. Cooperation between translating ribosomes and RNA polymerase in transcription elongation. Science. 2010; 328:504–508. Medline CrossRef. [PubMed: 20413502]

22. Donahue BA, Yin S, Taylor JS, Reines D, Hanawalt PC. Transcript cleavage by RNA polymerase II arrested by a cyclobutane pyrimidine dimer in the DNA template. Proc Natl Acad Sci USA. 1994; 91:8502–8506. Medline CrossRef. [PubMed: 8078911]

23. Selby CP, Drapkin R, Reinberg D, Sancar A. RNA polymerase II stalled at a thymine dimer: footprint and effect on excision repair. Nucleic Acids Res. 1997; 25:787–793. Medline CrossRef. [PubMed: 9016630]

24. Selby CP, Sancar A. Transcription preferentially inhibits nucleotide excision repair of the template DNA strand *in vitro*. J Biol Chem. 1990; 265:21330–21336. Medline. [PubMed: 2250027]

25. Manelyte L, Kim YI, Smith AJ, Smith RM, Savery NJ. rate enhancement during transcription-coupled DNA repair. Mol Cell. 2010; 40:714–724. Medline CrossRef. [PubMed: 21145481]

26. Batty DP, Wood RD. Damage recognition in nucleotide excision repair of DNA. Gene. 2000; 241:193–204. Medline CrossRef. [PubMed: 10675030]

27. Doudney CO, Rinaldi CN. Chloramphenicol-promoted increase in resistance to UV damage in *Escherichia coli* B/r WP2 trpE65: development of the capacity for successful repair of otherwise mutagenic or lethal lesions in DNA. Mutat Res. 1985; 143:29–34. Medline CrossRef. [PubMed: 3889602]

28. Hanawalt PC. The U.V. sensitivity of bacteria: its relation to the DNA replication cycle. Photochem Photobiol. 1966; 5:1–12. Medline CrossRef. [PubMed: 5340914]

29. Tomko EJ, et al. 5′-Single-stranded/duplex DNA junctions are loading sites for *E. coli* UvrD translocase. EMBO J. 2010; 29:3826–3839. Medline CrossRef. [PubMed: 20877334]

30. Korzheva N, et al. A structural model of transcription elongation. Science. 2000; 289:619–625. Medline CrossRef. [PubMed: 10915625]

31. Toulokhonov I, Artsimovitch I, Landick R. Allosteric control of RNA polymerase by a site that contacts nascent RNA hairpins. Science. 2001; 292:730–733. Medline CrossRef. [PubMed: 11326100]

32. Bar-Nahum G, et al. A ratchet mechanism of transcription elongation and its control. Cell. 2005; 120:183–193. Medline CrossRef. [PubMed: 15680325]

33. Ahn BA. physical interaction of UvrD with nucleotide excision repair protein UvrB. Mol Cells. 2000; 10:592–597. Medline CrossRef. [PubMed: 11101153]

34. Manelyte L, et al. The unstructured C-terminal extension of UvrD interacts with UvrB, but is dispensable for nucleotide excision repair. DNA Repair (Amst). 2009; 8:1300–1310. Medline CrossRef. [PubMed: 19762288]

35. Tornaletti S. Transcription arrest at DNA damage sites. Mutat Res. 2005; 577:131–145. Medline CrossRef. [PubMed: 15904937]

36. Trautinger BW, Jaktaji RP, Rusakova E, Lloyd RG. RNA polymerase modulators and DNA repair activities resolve conflicts between DNA replication and transcription. Mol Cell. 2005; 19:247–258. Medline CrossRef. [PubMed: 16039593]

37. Arthur HM, Eastlake PB. Transcriptional control of the *uvrD* gene of *Escherichia coli*. Gene. 1983; 25:309–316. Medline CrossRef. [PubMed: 6319240]

38. Maluf NK, Fischer CJ, Lohman TM. A dimer of *Escherichia coli* UvrD is the active form of the helicase *in vitro*. J Mol Biol. 2003; 325:913–935. Medline CrossRef. [PubMed: 12527299]

39. Dutta D, Shatalin K, Epshtein V, Gottesman ME, Nudler E. Linking RNA polymerase backtracking to genome instability in *E coli*. Cell. 2011; 146:533–543. Medline CrossRef. [PubMed: 21854980]

40. Witkin EM. Mutation and the repair of radiation damage in bacteria. Radiat Res. 1966; 6(suppl): 30–53. Medline CrossRef. [PubMed: 5334394]

41. Schalow BJ, Courcelle CT, Courcelle J. Mfd is required for rapid recovery of transcription following UV-induced DNA damage but not oxidative DNA damage in *Escherichia coli*. J Bacteriol. 2012; 194:2637–2645. Medline CrossRef. [PubMed: 22427630]

42. Brueckner F, Cramer P. DNA photodamage recognition by RNA polymerase II. FEBS Lett. 2007; 581:2757–2760. Medline CrossRef. [PubMed: 17521634]

43. Churchman LS, Weissman JS. Nascent transcript sequencing visualizes transcription at nucleotide resolution. Nature. 2011; 469:368–373. Medline CrossRef. [PubMed: 21248844]

44. Compe E, Egly JM. TFIIH: when transcription met DNA repair. Nature Rev Mol Cell Biol. 2012; 13:343–354. Medline CrossRef. [PubMed: 22572993]

45. Drapkin R, et al. Dual role of TFIIH in DNA excision repair and in transcription by RNA polymerase II. Nature. 1994; 368:769–772. Medline CrossRef. [PubMed: 8152490]

46. Yang B, et al. Identification of cross-linked peptides from complex samples. Nature Methods. 2012; 9:904–906. Medline CrossRef. [PubMed: 22772728]

47. Murakami KS. X-ray crystal structure of *Escherichia coli* RNA polymerase σ70 holoenzyme. J Biol Chem. 2013; 288:9126–9134. Medline CrossRef. [PubMed: 23389035]

48. Runyon GT, Wong I, Lohman TM. Overexpression, purification, DNA binding, and dimerization of the *Escherichia coli uvrD* gene product (helicase II). Biochemistry. 1993; 32:602–612. Medline CrossRef. [PubMed: 8380701]

49. Pakotiprapha D, Samuels M, Shen K, Hu JH, Jeruzalmi D. Structure and mechanism of the UvrA-UvrB DNA damage sensor. Nature Struct Mol Biol. 2012; 19:291–298. Medline CrossRef. [PubMed: 22307053]

50. Li D, et al. pFind: a novel database-searching software system for automated peptide and protein identification via tandem mass spectrometry. Bioinformatics. 2005; 21:3049–3050. Medline CrossRef. [PubMed: 15817687]

51. Lutz R, Bujard H. Independent and tight regulation of transcriptional units in *Escherichia coli* via the LacR/O, the TetR/O and AraC/I1-I2 regulatory elements. Nucleic Acids Res. 1997; 25:1203–1210. Medline CrossRef. [PubMed: 9092630]

52. Epshtein V, Toulme F, Rahmouni AR, Borukhov S, Nudler E. Transcription through the roadblocks: the role of RNA polymerase cooperation. EMBO J. 2003; 22:4719–4727. Medline CrossRef. [PubMed: 12970184]

53. Pósfai G, et al. Emergent properties of reduced-genome *Escherichia coli*. Science. 2006; 312:1044–1046. Medline CrossRef. [PubMed: 16645050]

54. Cardinale CJ, et al. Termination factor Rho and its cofactors NusA and NusG silence foreign DNA in *E. coli*. Science. 2008; 320:935–938. Medline CrossRef. [PubMed: 18487194]
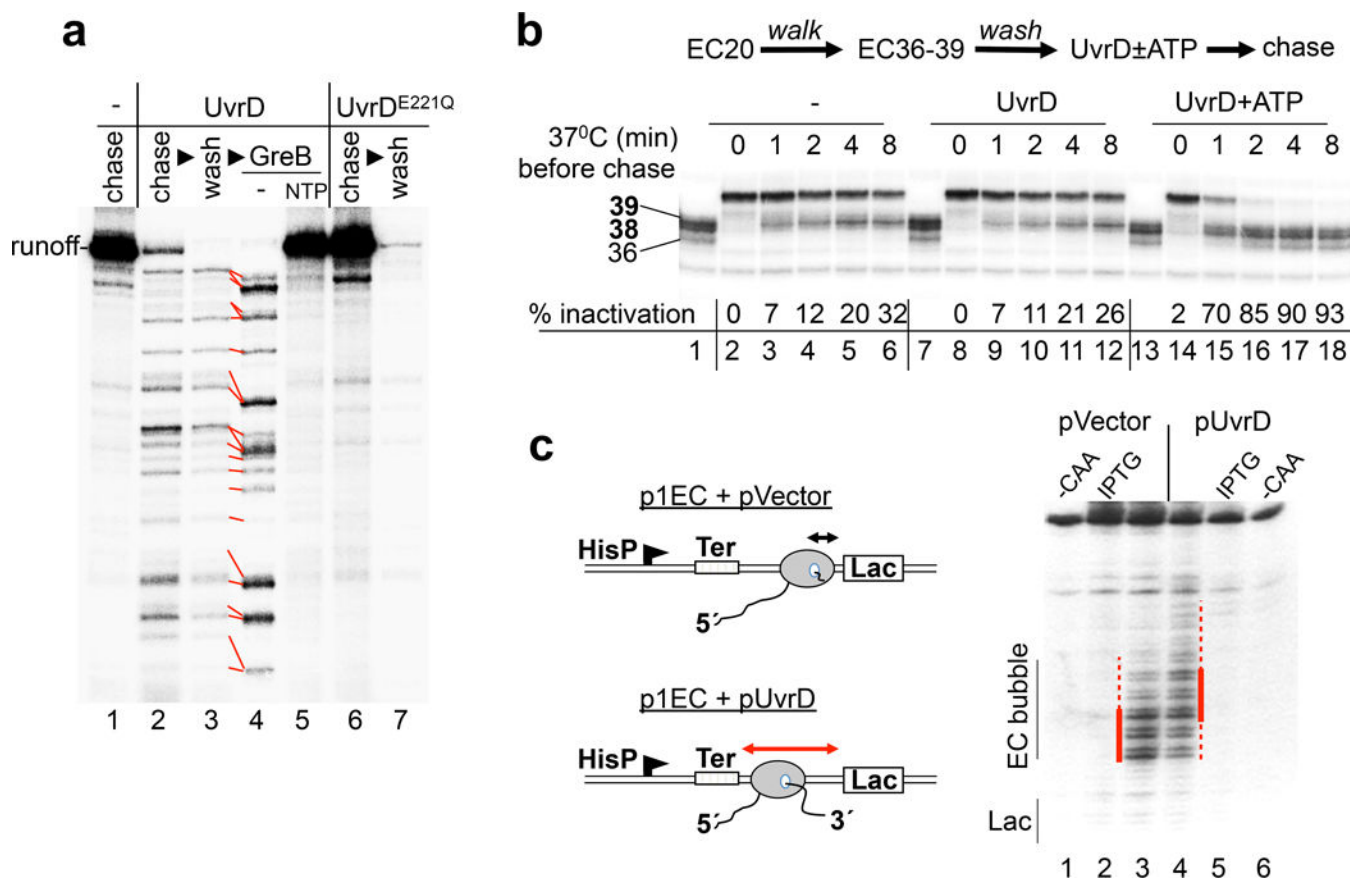
Figure 1. UvrD promotes RNAP backtracking

a, EC20 was combined with wild-type UvrD (lanes 2–5), catalytically inactive UvrD[E221Q], (lanes 6, 7), or no UvrD (lane 1) before NTP chase (lanes 1, 2, 6) and wash (lanes 3, 7). Red lines connect corresponding RNAs from arrested elongation complexes before and after GreB cleavage (lanes 4, 5). **b**, EC11 was walked to positions 36, 38 and 39. UvrD was added ± ATP and chased. Inactivated EC36–39 (%) is indicated. **c**, The p1EC constructs[21] (left) and primer extension analyses (right). CAA modifications on the non-template strand of p1EC + pVector (lanes 2, 3) or p1EC + pUvrD (lanes 4, 5). The lac operator (Lac) and transcription bubble are indicated. Red lines show elongation complex position.
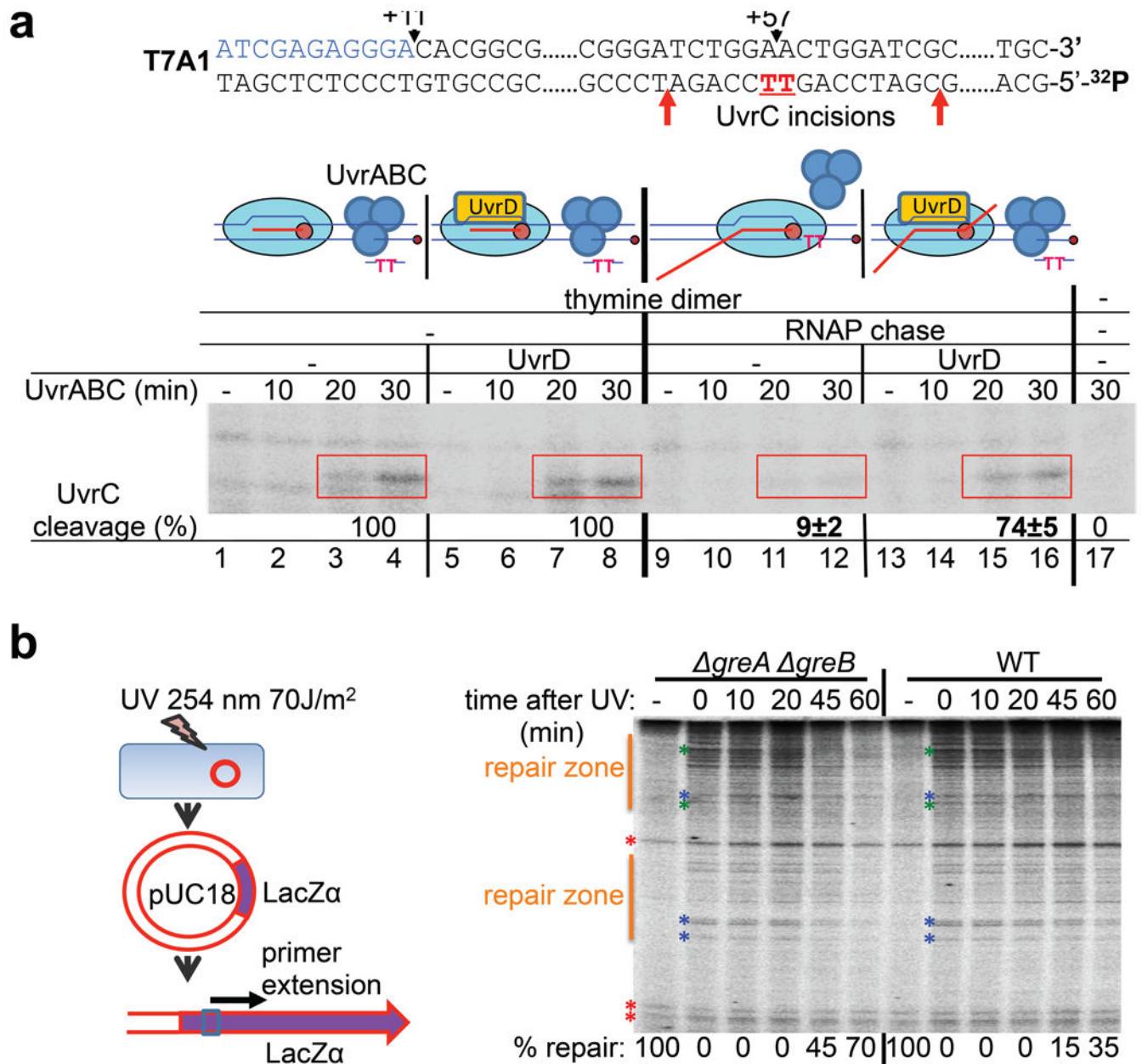
Figure 2. RNAP backtracking facilitates NER

a, UvrD pulls RNAP from thymine dimers (TT). The T7A1 promoter template with TT (red) and schematic overview (top); EC11 was chased to TT (lanes 9–16) (bottom). Where indicated, UvrD was added for 5 min. Red boxes show UvrC-mediated DNA cleavage products (19 nucleotides); per cent cleavage is averaged (± s.e.m.) from four independent experiments $P < 0.05$. **b**, Left, the primer extension experimental overview. Right, primer extension products reflect the location of lesions. Orange lines indicate repair zones for percentage repair. Asterisks indicate representative lesions repaired faster in *greAB* than in wild-type cells (blue), at the same rate (green) or 'non-disappearing' bands for normalization (orange).
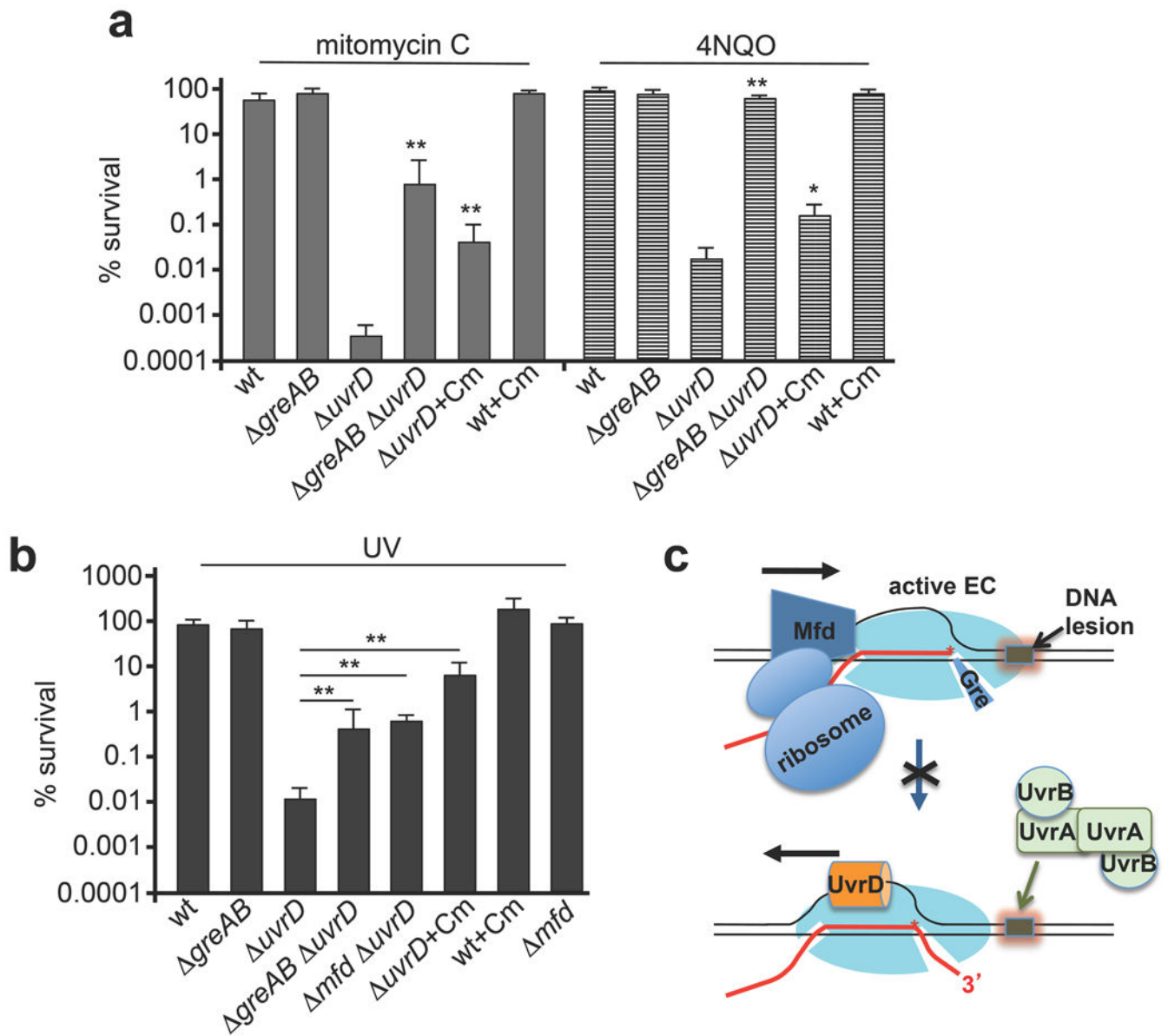
**Figure 3. Anti-backtracking factors obstruct UvrD activity in NER**

a, Inactivating *greAB* or slowing ribosomal translocation (with 1 μg ml^{-1} chloramphenicol) suppresses *uvrD* sensitivity to mitomycin C (1 μg ml^{-1}; filled bars) and 4NQO (1 μM; striped bars). Data from three independent experiments are presented as the mean ± s.e.m.; *P < 0.05, **P < 0.01. Cm, chloramphenicol; wt, wild type. **b**, Inactivating *greAB, mfd* or slowing ribosomal translocation suppresses *uvrD* sensitivity to UV irradiation (5 J per m^2 at 30 °C). Data from three independent experiments are presented as the mean ± s.e.m.; **P < 0.01. **c**, Cartoon summarizing interference with NER.
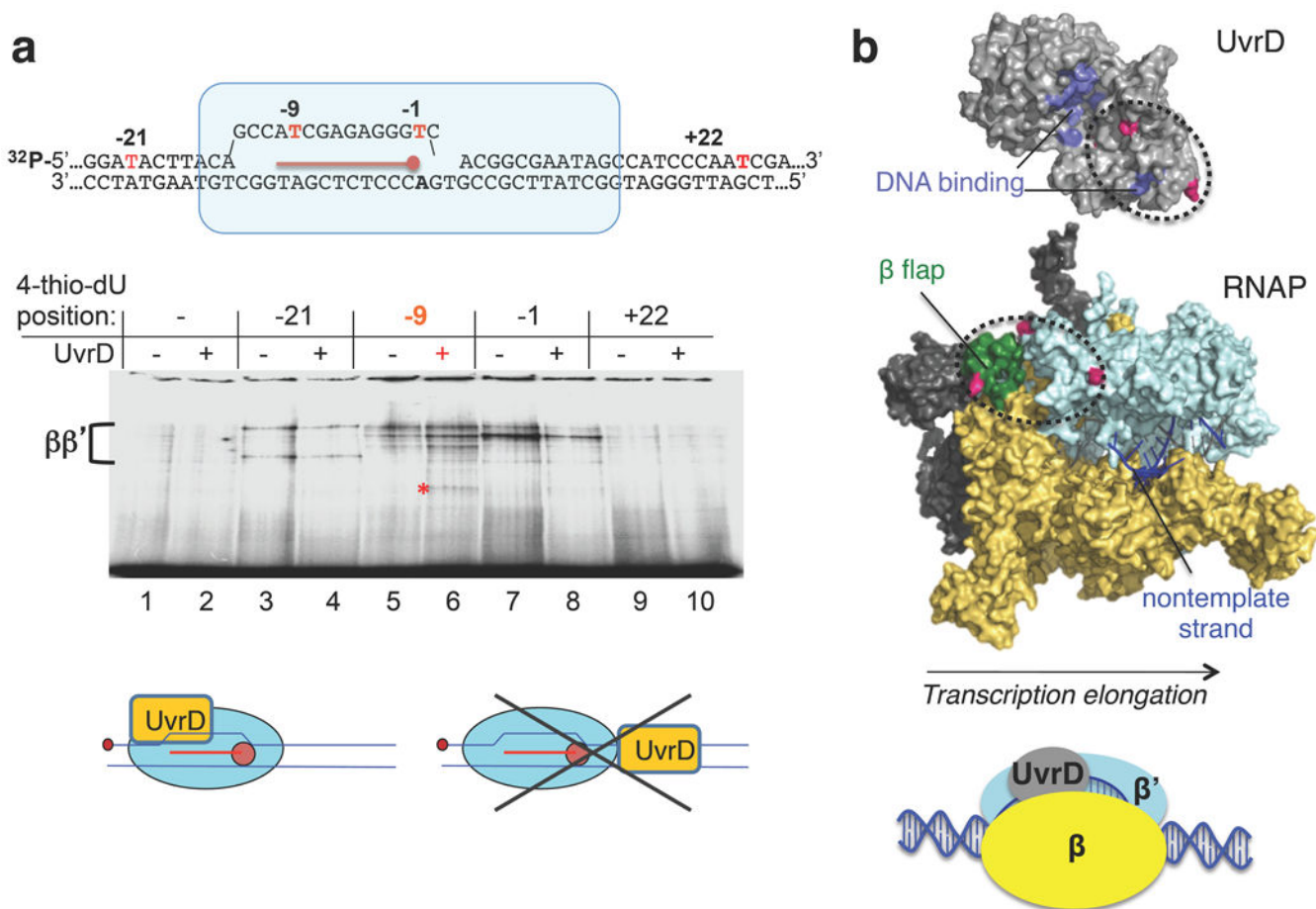
Figure 4. Mapping UvrD interactions with the elongation complex

a, The 5′-radiolabelled scaffold carries a single photo-inducible 4-thio-dU (red) in the template strand (top). Protein crosslinking adducts corresponding to the β and β′ subunits of RNAoP and UvrD (red asterisk) (middle). A model of UvrD binding (bottom). **b**, UvrD (top, Protein Data Bank (PDB) accession number 2IS4)[12] is cross-linked to RNAP (middle, PDB accession number 4IGC)[47] at three positions (magenta) that span the β (yellow) and β′ (light blue) subunits, proximal to the non-template strand (blue, PDB accession number 4G7O). The β flap-tip-helix (green) is indicated and the suggested binding interface is circled. Schematic summarizing UvrD–RNAP binding shown below.
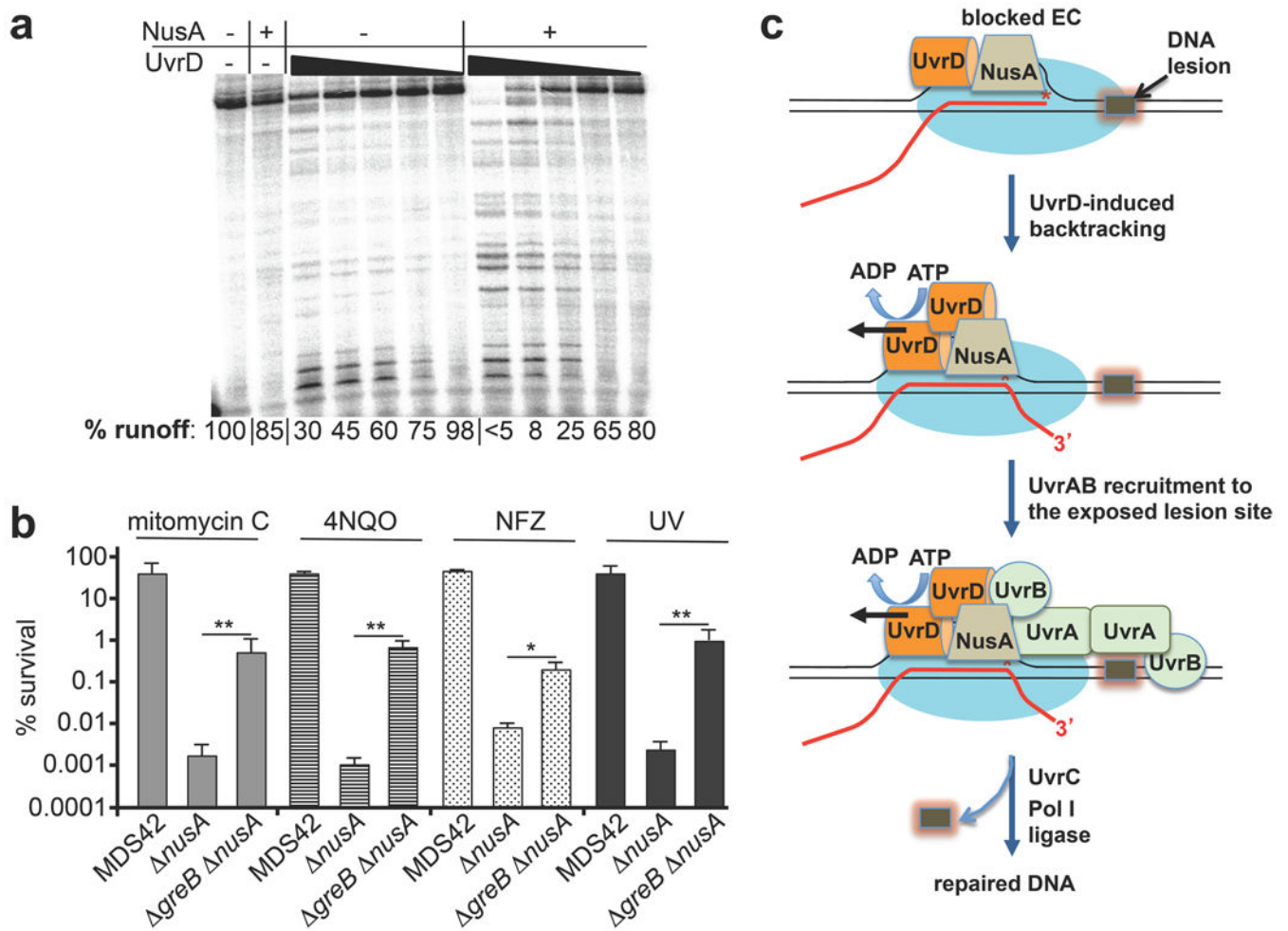
Figure 5. UvrD and NusA cooperate in backtracking-mediated NER

a, NusA facilitates UvrD-mediated backtracking. The fraction of full-length transcript (percentage runoff) is indicated. **b**, GreB inactivation in MDS43 cells suppresses *nusA* sensitivity to mitomycin C (0.5 μg ml^{-1}), 4NQO (3 μM), nitrofurazone (NFZ, 2 μM), and UV irradiation (15 J per m^2). Data from three independent experiments are presented as the mean ± s.e.m.; *$P < 0.05$, **$P < 0.01$. **c**, Model for backtracking-mediated NER.